Integrated Cubic Phase Function for Linear FM Signal Analysis

Pu Wang,Hongbin Li, Igor Djurović and Braham Himed

Abstract— **In this paper, an integrated cubic phase function (ICPF) is introduced for the estimation and detection of linear frequency-modulated (LFM) signals. The ICPF extends the standard cubic phase function (CPF) to handle cases involving low signal-to-noise ratio (SNR) and multi-component LFM signals. The asymptotic mean squared error (MSE) of an ICPF-based estimator as well as the output SNR of an ICPF-based detector are derived in closed-form and verified by computer simulation. Comparison with several existing approaches is also included, which shows that the ICPF serves as a good candidate for LFM signal analysis.**

I. Introduction

Frequency-modulated (FM) signals have many applications in radar, sonar, communications, and seismic analysis [1–4]. One important class of such signals are linear FM (LFM) signals frequently encountered in modern radar systems [3,4]. Due to target motion, radar return signals can be modeled as LFM signals whose parameters, e.g., initial frequencies and chirp-rates, reveal useful information about the target, i.e., its velocity and acceleration.

Detection and parameter estimation of LFM signals have received considerable attention in recent years [5–17]. Early efforts were focused on the analysis of single-component LFM signal. The maximum likelihood estimator (MLE), which is also called the generalized chirp transform (GCT) in [18], was examined in [5]. Although statistically optimal, the MLE requires a two-dimensional (2-D) joint maximization over the initial frequency and chirp-rate parameters and is computationally demanding. The MLE also requires accurate initial parameter estimates to avoid local maxima and a numerical search is performed by utilizing a Newton algorithm [5]. Suboptimal techniques are therefore desired for practical implementation. In [6], a phase unwrapping algorithm followed by least-square fitting was proposed, which is suitable for single-component LFM signal estimation at high signal-to-noise ratio (SNR). The discrete polynomial transform (DPT) was employed to reduce the 2-D maximization problem in the MLE to a one-dimensional (1-D) problem [7]. Time-frequency analysis was also studied for LFM signal estimation. For example, the Wigner-Ville distribution (WVD) can be used to track the time-varying frequency of the LFM signal. In general, these techniques can produce good results for single-component LFM signal at moderate to high SNR.

For multi-component LFM signals which arise in many applications, a number of techniques were proposed in [8–13, 16, 17]. The Cramér-Rao bound (CRB) and MLE for multi-component LFM signals were investigated in [10] and [17]. A combined Radon-WVD transform (RWT) was proposed to turn the task of tracking straight lines in the time-frequency domain into one of locating the maxima in a 2-D domain [8,9], which is still computationally complex due to the 2-D optimization. To reduce the 2-D problem into a 1-D problem, the Radon-Ambiguity transform (RAT) was proposed by exploiting the property that auto-terms in the ambiguity function pass through the origin of the ambiguity domain (also see Section III) [13]. It was shown that, compared with the RWT, the RAT provides comparable performance with reduced computation, especially in cases where the chirp-rate is the only parameter of interest. Nevertheless, the computational complexity remains high since the RAT requires an additional Cartesian-to-Polar coordinate transformation and interpolations.

Recently, an instantaneous frequency rate

IEEE Transactions on Aerospace and Electronics Systems, Vol. 45, No. 4, Dec. 2009.

(IFR) estimator, using the cubic phase function (CPF), was proposed for FM signal estimation [19]. The CPF-based approach is asymptotically efficient for single-component LFM signals [20]. However, for multi-component LFM signals, the CPF exhibits spurious peaks that cause an identifiability problem. The more the LFM components, the higher the occurrence probability of spurious peaks [16]. Hence, there is a need to develop robust techniques for the estimation and detection of multi-component LFM signals.

In this paper, an integrated cubic phase function (ICPF) is proposed for LFM signal estimation and detection. The ICPF exploits the property that the auto-terms in the CPF are distributed along straight lines parallel to the time axis in the time-"frequency rate" domain, and hence integrates over these lines to enhance the auto-terms (see Section II for an illustration of the auto-terms and spurious peaks). It is shown that, compared with the CPF, the ICPF can provide considerably lower mean squared error (MSE) at low SNR, lower SNR threshold, and better rejection of spurious peaks or cross-terms for multi-component LFM signals. Additionally, the ICPF is computationally more efficient than the RWT since the former involves a 1-D optimization, as opposed to a 2-D optimization used in the RWT. It is also more efficient than the RAT since the ICPF does not require the computationally expensive Cartesian-to-Polar coordinate transformation. The performance of the ICPF is examined in terms of the asymptotic MSE and output SNR.

The paper is organized as follows. The problem formulation is described in Section II. Section III introduces the definition of the ICPF. An ICPF-based parameter estimation for the LFM signal is proposed in Section IV. The asymptotic MSE of the ICPF-based estimates is also included in this Section. Section V proposes an ICPF-based detector and its performance is characterized in terms of the output SNR and the SNR threshold. Numerical examples are provided in Section VI. Finally, conclusions are drawn in Section VII.

II. Problem Formulation

Consider noise-contaminated observations of a K-component LFM signal:

$$x(n) = \sum_{k=1}^{K} s_k(n) + v(n)$$

$$= \sum_{k=1}^{K} A_k \exp\left\{j(a_{k,0} + a_{k,1}n + a_{k,2}n^2)\right\} + v(n),$$

$$n \in \mathbb{Z} \triangleq \{\ltimes_{\nu}, \ltimes_{\nu} + \nVdash, \cdots, \ltimes_{\nu} + \mathbb{N} - \nVdash\}, \tag{1}$$

where $A_k, a_{k,0}, a_{k,1}$, and $a_{k,2}$ denote the unknown amplitude, phase parameter, frequency parameter, and chirp-rate parameter for the kth component, respectively, which are to be estimated, n_0 is the initial time index, N is the number of temporal samples, and the noise $v(n)$ is assumed to be a complex white Gaussian noise with zero-mean and variance σ^2. Historically, two cases have been considered for the initial time index n_0, i.e., $n_0 = 0$ and $n_0 = -(N-1)/2$ (assume N is odd), respectively. Note that the two choices lead to different LFM signals since the instantaneous frequencies are different. Here, we do no fix the value of n_0 so that we can address both cases. To avoid ambiguities arising from the cyclic nature of spectral transforms of sampled signals, it is assumed that [21, 22]

$$\begin{aligned} |a_1| &\leq \pi, \\ |a_2| &\leq \pi/N. \end{aligned} \tag{2}$$

The CPF, which was introduced to extract the IFR [19], is defined as

$$\mathrm{CPF}(n, \Omega) = \sum_{m} x(n+m)x(n-m)e^{-j\Omega m^2},$$

$$m \in \mathbb{L} \triangleq \{\lambda : n + \lambda \in \mathbb{Z}, n - \lambda \in \mathbb{Z}\}, \tag{3}$$

where Ω represents the IFR index for the spectrum of the CPF. It is noted that the CPF concentrates the LFM signal energy along straight lines $\Omega = 2a_{k,2}$ in the $(n-\Omega)$ (time-"frequency rate") domain. For comparison, Fig. 1 (a)-(c) plot the Wigner-Ville distribution, Ambiguity Function and CPF, respectively, of a 2-component LFM signal with parameters $A_1 =$

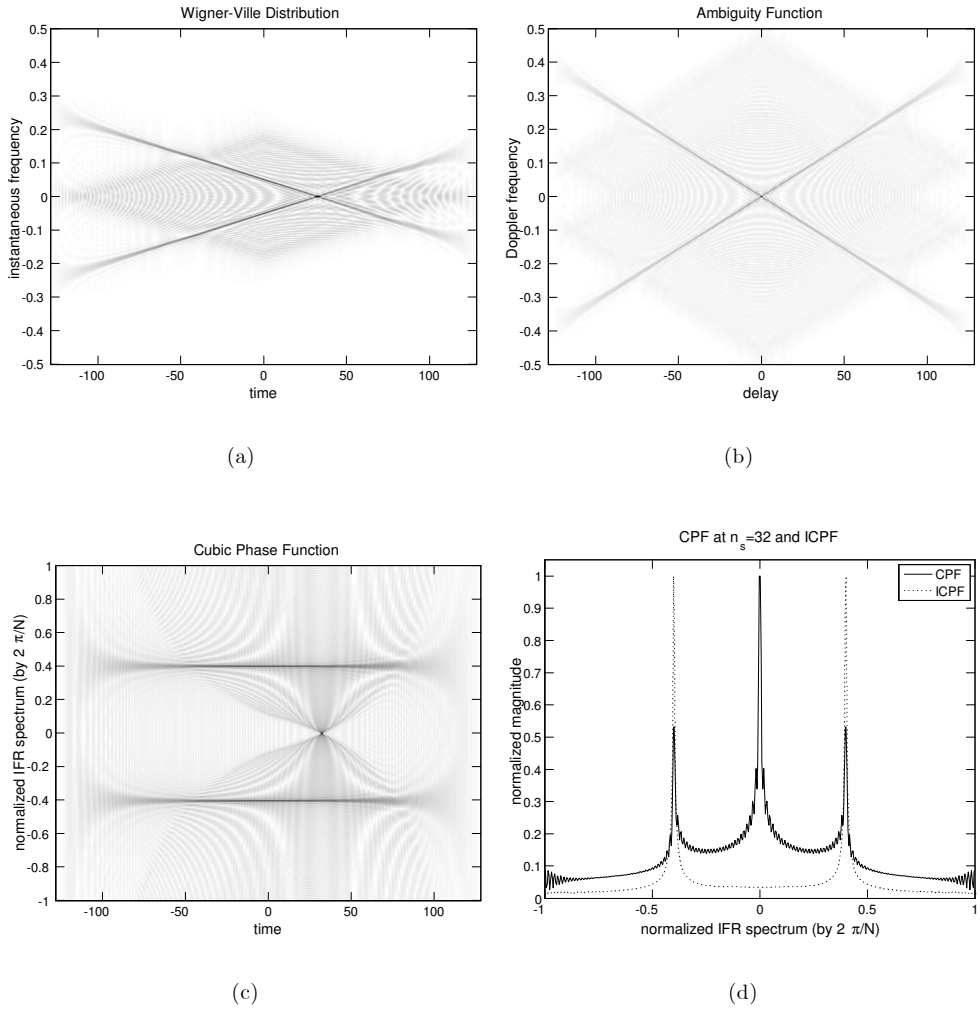

Fig. 1. The Wigner-Ville distribution (WVD), Ambiguity Function (AF) and Cubic Phase Function (CPF) of a 2-component LFM signals.

$A_2 = 1$, $a_{1,0} = a_{2,0} = 0$, $a_{2,1} = -a_{1,1} = 0.1\pi$, $a_{1,2} = -a_{2,2} = 0.4\pi/N$, and $N = 257$.

The CPF is asymptotically efficient for parameter estimate of a single-component LFM signal estimation [20]. However, an identifiability problem occurs due to cross-terms and spurious peaks when dealing with multi-component LFM signals [16]. For example, consider a 2-component LFM signal

$$x(n) = A_1 \exp\{j(\underbrace{a_{1,0} + a_{1,1}n + a_{1,2}n^2}_{\phi_1(n)})\}$$
$$+A_2 \exp\{j(\underbrace{a_{2,0} + a_{2,1}n + a_{2,2}n^2}_{\phi_2(n)})\}, \qquad (4)$$

where the observation noise is ignored for simplicity. The bilinear transform in the CPF results in

$$x(t+m)x(t-m) =$$
$$= \underbrace{A_1^2 e^{j2\phi_1(n)} e^{j2a_{1,2}m^2} + A_2^2 e^{j2\phi_2(n)} e^{j2a_{2,2}m^2}}_{\text{auto-terms}}$$
$$+ \underbrace{A_1 A_2 e^{j(\phi_1(n)+\phi_2(n))} e^{j\left[(a_{1,2}+a_{2,2})m^2+\rho(n)m\right]}}_{\text{cross-term 1}}$$

$$+\underbrace{A_1A_2e^{j(\phi_1(n)+\phi_2(n))}e^{j\left[(a_{1,2}+a_{2,2})m^2-\rho(n)m\right]}}_{\text{cross-term 2}}, \tag{5}$$

where

$$\rho(n) = (a_{1,1} - a_{2,1}) + 2\,(a_{1,2} - a_{2,2})\,n. \tag{6}$$

The auto-terms in (5) exhibit a quadratic phase in m, whereas the cross-terms have both linear and quadratic phases in m with coefficient related to the time index n. By applying the quadratic phase filtering, i.e., $\sum_m(\cdot)e^{-j\Omega m^2}$, the auto-terms are localized along two straight lines independent of the time index, i.e., $\Omega = 2a_{1,2}$ and $\Omega = 2a_{2,2}$, while the cross-terms are distributed along trajectories varying with time (see Fig. 1(c)).

However, when $\rho(n) = 0$ (see (6)), the two hybrid phase terms in m reduce to a quadratic phase terms in m, and (5) reduces to

$$x(n+m)x(n-m) =$$
$$= \underbrace{A_1^2e^{j2\phi_1(n)}e^{j2a_{1,2}m^2} + A_2^2e^{j2\phi_2(n)}e^{j2a_{2,2}m^2}}_{\text{auto-terms}}$$
$$+\underbrace{2A_1A_2e^{j(\phi_1(n)+\phi_2(n))}e^{j(a_{1,2}+a_{2,2})m^2}}_{\text{spurious peak}}. \tag{7}$$

After the quadratic phase filtering, the two cross-terms converge into a single peak at the time index n_s such that $\rho(n_s) = 0$. For the 2-component LFM signal in Fig. 1(c), $n_s \approx 32$. Fig. 1(d) shows a slice of the CPF at $n_s = 32$. It is observed that the highest peak is the spurious peak at $\Omega = a_{1,2} + a_{2,2}$. The situation becomes worse in dense LFM signal environments. Specifically, for a K-component LFM signal, there are $(K^2 - K)$ cross-terms which may lead to up to $(K^2 - K)/2$ spurious peaks [16].

III. The Integrated Cubic Phase Function

To address the above identifiability problem of the CPF, it is desirable to separate the auto-terms from the cross-terms and spurious peaks. By reviewing (5) and (7), we observe that the auto-terms of the CPF are distributed over straight lines parallel to the time axis, whereas the locations of the cross-terms vary with time and the spurious peaks occur at discrete locations that are subject to the constraint (6). This property motivates us to integrate along straight lines parallel to the time to enhance the energy of the auto-terms. Once the integral path matches the location of an auto-term, the integral adds up the energy of the auto-terms, thus forming a peak that can be exploited to simplify the detection and estimation of LFM signals.

Specifically, the integral path for the CPF is shown in Fig. 2 (c). For comparison, Fig. 2 includes the integral path for the RWT [8] and RAT [13], respectively, where the dash line shows the integral path that is uniquely determined by the rotation angle θ, or the integral radius r, or both. In particular, the RWT needs to integrate all straight lines in the time-frequency domain by varying the values of both θ and r, while the RAT just integrates straight lines passing through the origin of the ambiguity domain (delay-"Doppler frequency" domain, equivalently) by fixing $r = 0$ and varying θ.

In this paper, the integrated cubic phase function (ICPF) is defined as follows

$$\text{ICPF}(\Omega) = \sum_n |\text{CPF}(n,\Omega)|^2$$
$$= \sum_n \sum_m \sum_l x(n+m)x(n-m)$$
$$\times x^*(n+l)x^*(n-l)e^{-j\Omega\left(m^2-l^2\right)}, \tag{8}$$

where m and l are drawn from the set $\mathbb{L}$ defined in (3). By direct substitution of an LFM signal into the above equation, the ICPF exhibits a peak at $\Omega = 2a_2$. This implies that the detection and parameter estimation of a noisy LFM signal can be performed through a 1-D search of the IFR spectrum. For multi-component LFM signals, the ICPF presents multiple peaks for the auto-terms and suppresses the cross-terms and spurious peaks. The ICPF for the 2-component LFM signal of Fig. 1(c) is shown in Fig. 1(d) in dotted line. It is observed that two distinct peaks corresponding to the auto-terms are shown, and the spurious peak is suppressed.

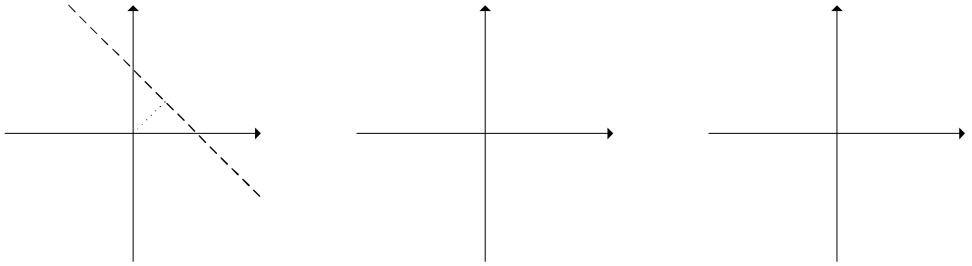

Fig. 2. The integral path for the RWT, RAT and ICPF over different 2-D domains, where θ and r denote the rotation angle and integral radius, respectively.

IV. An ICPF-Based Parameter Estimation

As shown in Fig. 1(d), the locations of the spectrum peaks is proportional to the chirp-rate parameters. Therefore, an ICPF-based estimator for the LFM parameters is introduced in the following.

A. Estimation Algorithm

By searching for peaks in the IFR spectrum, the chirp-rate parameters for the LFM signal can be estimated. For multi-component LFM signals, we can estimate one chirp-rate parameter at a time. Once an estimate of $a_{k,2}$ is obtained, a dechirping technique is used to convert the observations $x(n)$ to a sinusoidal signal, and the remaining parameters for the estimated LFM signal are obtained using the following procedure:

1) Dechirp: $x_d(n) = x(n)e^{-j\hat{a}_{k,2}n^2}$;

2) Estimate $a_{k,1}$ by DFT:

$$\hat{a}_{k,1} = \arg\max_{\omega} X_d(\omega), \tag{9}$$

where $X_d(\omega) = \left|\sum_n x_d(n)e^{-j\omega n}\right|^2$.

3) Estimate $a_{k,0}$ and A_k by least-square: let $y_d(n) = x_d(n)e^{-j\hat{a}_{k,1}n}$,

$$\hat{a}_{k,0} = \text{angle}\left[\frac{1}{N}\sum_n y_d(n)\right] = \Im\left\{\log\left[\frac{1}{N}\sum_n y_d(n)\right]\right\}, \tag{10}$$

$$\hat{A}_k = \frac{1}{N}\sum_n y_d(n)e^{-j\hat{a}_{k,0}} = e^{\Re\left\{\log\left[\frac{1}{N}\sum_n y_d(n)\right]\right\}}, \tag{11}$$

where $\Im\{\cdot\}$ and $\Re\{\cdot\}$ denote the imaginary and real parts of $\{\cdot\}$, respectively. The second equality in (10) and (11) shown in [7] will be used in Appendix I for performance analysis.

4) Cancel out the estimated LFM signal using $x(n) = x(n) - \hat{A}_k e^{j(\hat{a}_{k,0}+\hat{a}_{k,1}n+\hat{a}_{k,2}n^2)}$, set $k = k+1$, and repeat steps 1)-4) until $k = K$.

To further improve the estimates, a refining step is helpful to reduce the estimation error caused by interference among different components of the LFM signal. An approach suggested in [11] is adopted here. Specifically, when all parameter estimates are obtained using the above procedure, we re-estimate the parameters of each LFM component by canceling out all LFM components other than the one to be estimated and repeating (8) and steps 1)-3).

B. Accuracy of The Estimation

In this section, the ICPF-based estimator is examined in terms of its asymptotic bias and MSE. In addition to the chirp-rate parameter estimate, we also study the accuracy of the

other parameter estimates, i.e., phase parameter a_0, frequency parameter a_1 and amplitude A, which are affected by the a_2 estimate error when the dechirping technique is used.

An exact analysis of the proposed ICPF-based LFM signal estimator for the multi-component case is difficult due to the interference among different LFM components caused by the non-linear operation of the ICPF. Note that by estimating one component at a time and interference cancelation (as described in Section III), our estimator effectively converts the problem into a series of single-component LFM signal estimation. In the sequel, we present an analysis for the single-component case, which provides a lower bound on the achievable performance of our estimator, subject to residual interference and imperfect cancelation. Computer simulation shows that the analysis is accurate even for relatively small values of N.

We employ a first-order perturbation analysis similar to the one of [7] for LFM signal estimation. This method is valid for high SNR and for a large number of samples. A SNR threshold effect usually occurs when the high SNR assumption is not met, and the Monte-Carlo simulation can be utilized to verify the theoretical analysis. For the ICPF estimate of the chirp-rate parameter, the first-order perturbation analysis is presented in Appendix A-A. The results show that the a_2 estimate is asymptotically unbiased, i.e., $\mathrm{E}\{\delta a_2\} = 0$, where δa_2 denotes the estimation error, and the corresponding asymptotic MSE is

$$E\left\{(\delta a_2)^2\right\} = \frac{90}{N^5}\left(\frac{1.008}{\mathrm{SNR}} + \frac{7.433}{\mathrm{SNR}^2 N}\right). \tag{12}$$

Once we have obtained the estimate of the chirp-rate parameter, according to the estimation procedure in Section III, the dechirping technique is applied and the remaining parameters are estimated using (9), (10) and (11). During this procedure, the error in the a_2 estimate may propagate to the other estimates, i.e., $\hat{a}_1, \hat{a}_0$ and $\hat{A}$. The error propagation effect is considered here. The derivation of the asymptotic bias and MSE of these estimates is presented in detail in Appendix A-B and A-C. It is shown that all estimates are asymptotically unbiased. Table I summarizes the asymptotic MSE of these estimates and the corresponding CRBs, which shows that the ICPF-based estimation is asymptotically efficient for the a_1 and A estimates, and approximately efficient for the a_2 and a_0 estimates at high SNR.

We note that similar observations, i.e., some parameters associated with the LFM signal are asymptotically efficient while the others are not, have been made in other non-linear LFM signal estimators (see, e.g., [7,23,24]). We also note that the MSE of different parameters decreases with N in different orders. For example, the MSE of $\hat{a}_2$ decreases as $1/N^5$ while the MSE of $\hat{a}_1$ decreases as $1/N^3$. Only the highest order of N is counted in each case for the asymptotic analysis.

V. The ICPF-Based Detection

LFM signal detection in the presence of noise using the proposed ICPF is considered in this section. Performance analysis of the ICPF-based detector is examined in terms of output SNR as well as the computational complexity.

A. ICPF-Based Detector

Consider the following binary hypothesis testing problem:

$$\begin{aligned} H_0 &: x(n) = v(n), \\ H_1 &: x(n) = s(n) + v(n) \\ &\qquad = Ae^{j(a_0 + a_1 n + a_2 n^2)} + v(n), \end{aligned} \tag{13}$$

where the LFM signal under H_1 has unknown parameters A, a_0, a_1, and a_2, and $v(n)$ is again white Gaussian noise with mean zero and known variance σ^2. A well-known detector for this problem is the generalized likelihood ratio test (GLRT) which substitutes the MLE of the unknown parameters under the alternative hypothesis into the likelihood ratio test [7]

$$T_{\mathrm{GLR}} = \left| \frac{1}{N} \sum_n x(n) e^{-j\hat{a}_{1,\,\mathrm{ML}} n - j\hat{a}_{2,\,\mathrm{ML}} n^2} \right| \underset{H_0}{\overset{H_1}{\gtrless}} \gamma_{\mathrm{GLR}}, \tag{14}$$

TABLE I
ASYMPTOTIC MSE AND CRB

The estimates	Asymptotic MSE	CRB
$\hat{a}_2$	$\frac{90}{N^5\mathrm{SNR}}\left(1.008+\frac{7.433}{N\mathrm{SNR}}\right)$	$\frac{90}{N^5\mathrm{SNR}}$
$\hat{a}_1$	$\frac{6}{N^3\mathrm{SNR}}\left(1+\frac{4}{N\mathrm{SNR}}\right)$	$\frac{6}{N^3\mathrm{SNR}}$
$\hat{a}_0$	$\frac{1.125}{N\mathrm{SNR}}\left(1.004+\frac{4.133}{N\mathrm{SNR}}\right)$	$\frac{1.125}{N\mathrm{SNR}}$
$\hat{A}$	$\frac{\sigma^2}{2N}$	$\frac{\sigma^2}{2N}$

where $\hat{a}_{1,\,\mathrm{ML}}$ and $\hat{a}_{2,\,\mathrm{ML}}$ denote the MLE of the a_1 and a_2, respectively, and γ_{GLR} is the detection threshold which is subject to a specified probability of false alarm. As stated in Section I, the MLE of the a_1 and a_2 requires a 2-D grid search and is also subject to local convergence problem. In [25], it is shown that the GLRT is equivalent to the RWT-based detection, which computes 2-D polar line integrals of the WVD

$$T_{\mathrm{RWT}} = \max_{\{\omega_0,\rho\}} \sum_n W(n,\omega_0+\rho n) \underset{H_0}{\overset{H_1}{\gtrless}} \gamma_{\mathrm{RWT}}, \tag{15}$$

where $W(n,\omega)$ denotes the WVD of $x(n)$ and γ_{RWT} is the RWT-based test threshold.

In practice, it is often the case that the chirp rate is the only parameter of interest e.g., detection of a small fast moving missile launched from a relatively slow moving aircraft [13]. In these cases, the 2-D approach still needs to perform a 2-D search. To simplify the 2-D detection approach, the RAT-based test realizes that the ambiguity function of $x(n)$ is distributed along a line going through the origin of the ambiguity plan and, therefore, computes only a 1-D Polar line integral

$$T_{\mathrm{RAT}} = \max_{\{\rho\}} \sum_\tau \left|Q(\tau,\rho\tau)\right|^2 \underset{H_0}{\overset{H_1}{\gtrless}} \gamma_{\mathrm{RAT}}, \tag{16}$$

where $Q(n,\omega)$ denotes the ambiguity function of $x(n)$ and γ_{RAT} is the RAT-based test threshold. Although the RAT-based test is a 1-D approach, the computation of the RAT still remains high due to the inherent Cartesian-to-Polar coordinate transformation and the 2-D interpolation.

In the following, an LFM signal detector, which is computationally more efficient than the above detectors, is introduced by using the proposed ICPF. By recalling that the ICPF concentrates the LFM signal to a peak in the IFR spectrum, we can decide the presence of the LFM signal by searching for peaks in the IFR spectrum exceeding a certain threshold. An ICPF-based detector is thus introduced by simply computing the ICPF and comparing the highest peak with a threshold:

$$T_{\mathrm{ICPF}} = \max_{\{\Omega\}} \sum_n \left|\mathrm{CPF}(n,\Omega)\right|^2 \underset{H_0}{\overset{H_1}{\gtrless}} \gamma_{\mathrm{ICPF}}, \tag{17}$$

where γ_{ICPF} is the corresponding detection threshold. From (17), the ICPF-based test is a 1-D approach, as opposed to the 2-D nature of the GLRT/RWT-based test, and involves only a 1-D Cartesian line integral, which does not require the Cartesian-to-Polar coordinate transformation and the 2-D interpolation of the RAT-based test. As a result, the ICPF-based test appears to be the most computationally efficient approach to detect an LFM signal (see Section V-C for more details).

B. Performance Metrics For Detection

In general, the distribution of the test statistic T_{ICPF} cannot be obtained in closed form due to the non-linear operation involved. For practical applications, the histogram of T_{ICPF} needs to be estimated from either experimental or simulated data to set the test threshold

γ_{ICPF}. Similarly, the probability of detection cannot be analytically expressed due to the non-linear transformation. Alternatively, the performance in terms of the probability of detection for a given probability of false alarm is determined by Monte-Carlo simulations and the results are shown in Section VI.

Another quantity used to characterize the performance of a detector is the output SNR, which is the ratio of the output signal power to the output noise power. In the absence of noise, i.e., $x(n) = s(n)$, the test statistic of the ICPF-based detector at the maximum point $\Omega_0 = 2a_2$ is denoted by $\text{ICPF}_s(\Omega_0)$. In the presence of noise, $x(n) = s(n) + v(n)$, the test statistic at Ω_0 is a random variable and is denoted as $\text{ICPF}_x(\Omega_0)$. As a result, the SNR output is defined as [9]

$$\text{SNR}_{\text{out}} = \frac{|\text{ICPF}_s(\Omega_0)|^2}{\text{var}\{\text{ICPF}_x(\Omega_0)\}}, \qquad (18)$$

where $\text{var}\{\cdot\}$ denotes the variance of its argument. Here, the input SNR is defined as $\text{SNR}_{\text{in}} = A^2/\sigma^2$. The output SNR for the ICPF-based detector is derived in Appendix B:

$$\text{SNR}_{\text{out}} = \frac{\text{SNR}_{\text{in}}^3 N^3}{8.1\text{SNR}_{\text{in}}^2 N^2 + 70.5N\text{SNR}_{\text{in}} + 192 + 36\text{SNR}_{\text{in}}^{-1}} \cdot \qquad (19)$$

At high input SNR, the above output SNR can be approximated by $\text{SNR}_{\text{out}} = \text{SNR}_{\text{in}}N/8.1$. For comparison, the output SNR of the squared form of the RWT-based and RAT-based detectors were shown in (47) of [13].

C. Computational Complexity

The computational complexity of the RWT-based, RAT-based and ICPF-based detectors is examined here. Let N be the number of temporal samples and M the number of samples in the transformation domain, where M is generally chosen larger than N to help locate the peak [8, 13]. The computational cost of the three detectors is listed in Table II, where RWT_1 denotes the RWT with direct implementation and RWT_2 the one using a dechirping-based implementation [8]. From Table II, the ICPF is seen to be more efficient than the RWT_1 and the RAT since the ICPF avoids the non-linear Cartesian-to-Polar coordinate transformation and the 2-D interpolation which is required in the RWT_1 and RAT. The RWT_2 and ICPF require a similar number of multiplications and additions. However, the ICPF requires only a 1-D maximization, compared with the 2-D maximization used by the RWT_2. Note that even if the chirp-rate parameter is the only parameter of interest, the RWT_2 still needs to search a 2-D (chirp-rate and frequency parameters) domain to find the peaks, while the ICPF implements only a 1-D search over the chirp-rate parameter.

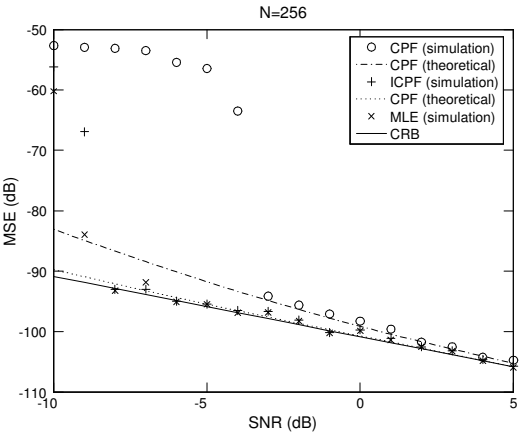

Fig. 3. MSE for the CPF and the ICPF versus SNR, when $N = 256$.

D. Threshold Analysis

Based on the output SNR, we can determine the input SNR threshold for the ICPF-based approach. In general, non-linear estimators often exhibit a threshold effect [26]. That is, at an SNR below a certain threshold, the first-order perturbation analysis, which is based on the assumption of high SNR, is no longer accurate. There are a number of ways to define the SNR threshold (see [7, 23, 24]). From a detection point of view, we define the SNR threshold as the input SNR which results in an output SNR exceeding a preset threshold (e.g., about 13-14 dB for high-resolution radars [1]). With the availability of the output SNR, the SNR

TABLE II
COMPARISON OF COMPUTATIONAL COMPLEXITY

Operation	RWT_1	RWT_2	RAT	ICPF
Multiplications	C_1	C_2	C_2	C_2
Additions	C_1	C_2	C_2	C_2
Coordinate Trans.	C_1	0	C_1	0
Interpolation	Yes	No	Yes	No
Maximization	2-D	2-D	1-D	1-D

$C_1 : O(MN^2)$.
$C_2 : O(MN \log_2 N)$.
The computational complexity of the CPF is $O(N \log_2 N)$ [19].

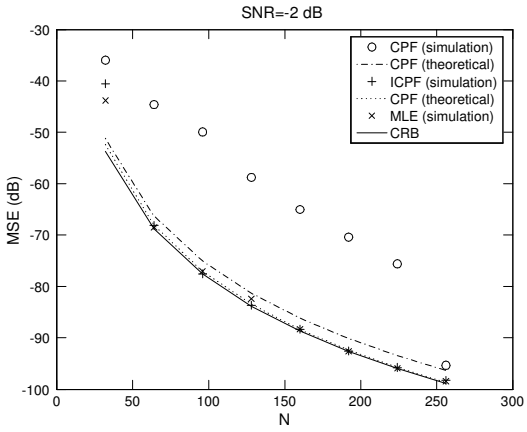

Fig. 4. MSE versus N for the a_2 estimate, when SNR $= -2$ dB.

threshold of the ICPF-based approach is given by (assuming a preset threshold of 14 dB):

$$\text{SNR}_t^{\text{ICPF}} = 10 \log_{10} \left(\frac{45}{N} \right). \qquad (20)$$

For a given input SNR, the SNR threshold for the ICPF-based approach decreases as the number of samples increases. The theoretical output SNR in (20) will be examined in a number of examples in Section VI.

VI. Numerical Examples

In this section, numerical examples are provided to illutrate the performance of the proposed methods and verify the theoretical results.

A. Single-Component LFM Signal Estimation

For a single-component LFM signal embedded in white Gaussian noise, the ICPF-based estimates have a lower SNR threshold and smaller MSE than those of the CPF-based estimates. To show this, a single-component LFM signal with parameters $A_1 = 1$, $(a_{1,0}, a_{1,1}, a_{1,2}) = (0, 0.2\pi, 0.22\pi/N)$, $n_0 = -(N-1)/2$, and $N = 256$ is considered. Fig. 3 shows the Monte-Carlo simulation results for the a_2 estimate using the CPF-based estimator, ICPF-based estimator, and the MLE. In simulations, the MLE is implemented in two steps: a coarse 2-D grid search followed by the Newton algorithm [5]. It is seen that the simulated MSE conforms to the theoretical MSE for the ICPF-based estimator. Moreover, the ICPF-based estimate produces lower MSE than the CPF-based estimates at low SNR, especially below -3 dB. The SNR threshold for the ICPF-based estimator is around -8 dB, as predicted by (20), which is 5 dB lower than that of the CPF-based estimator around -3 dB. In addition, it is shown that the ICPF-based estimator has almost identical performance with the MLE above the ICPF-based SNR threshold.

Fig. 4 shows the MSE of the a_2 estimate with the corresponding CRB [27] as the number of samples N increases. The other parameters are the same as in the previous example. At SNR $= -2$ dB, the CPF-based estimator works only when N is fairly large, while the ICPF-based estimator and the MLE provides

lower MSE at smaller N. Moreover, it is seen that the ICPF estimate of a_2 is nearly efficient for most values of N considered here, whereas the CPF-based estimator has a noticeable gap to the CRB even after the threshold effect disappears.

With a similar performance as the MLE, the ICPF-based estimator is beneficial from the viewpoint of complexity. In implementing the MLE, a brute force 2-D grid search is required to locate the convergence region around the optimum. As opposed to the 2-D maximization and search of the MLE, the ICPF-based estimator needs only a 1-D search to estimate the chirp-rate parameter. In addition, as shown in the Figs. 3 and 4, once the initial estimate of the MLE is out of the convergence region, the MLE converges to local maxima and achieves worse performance.

B. Multi-Component LFM Signals Estimation

A 2-component LFM signal embedded in complex white Gaussian noise is considered. The parameters of the 2-component LFM signal are $A_1 = A_2 = 1$, $(a_{1,0}, a_{1,1}, a_{1,2}) = (0, 0.2\pi, 0.22\pi/N)$, $(a_{2,0}, a_{2,1}, a_{2,2}) = (0, 0.8\pi, -0.31\pi/N)$, $n_0 = 0$, and $N = 64$ [17]. To reduce estimation bias, as we mentioned in Section III, a refining estimation step is performed by canceling out all other components except the one to be estimated. The MSE of the ICPF-based estimates is seen to match well by the theoretical MSE obtained in Section IV. The MSE is also compared with the CRB corresponding to the case of multi-component LFM signal [10, 17]. The performance of the multi-component MLE was shown in [17].

Fig. 5(a) shows the MSE for the first component of the LFM signal, using the CPF-based and ICPF-based estimators, respectively. It is shown that the SNR threshold of the ICPF-based estimate is around -1 dB, which agrees with the analytical result in (20). At an SNR above the threshold, the MSE for the ICPF-based estimate is close to the theoretical MSE. For the CPF-based estimation, the time index is chosen at $n = 36$, where spurious peaks appear according to $\rho(n) = 0$ in (6). Compared with the ICPF-based estimate, the CPF-based estimate is worse due to interference, including cross-terms and spurious peaks, even at high SNR.

A more challenging case involving a 5-component LFM signal with varying SNRs and close chirp-rates is considered next. Specifically, the ith component SNR is defined as A_i^2/σ^2. The LFM signal parameters are $(A_1, a_{1,0}, a_{1,1}, a_{1,2}) = (1, 0, 0.2\pi, 0.4\pi/N)$, $(A_2, a_{2,0}, a_{2,1}, a_{2,2}) = (0.5, 0, 0.1\pi, 0.1\pi/N)$, $(A_3, a_{3,0}, a_{3,1}, a_{3,2}) = (0.25, 0, 0.4\pi, 0.3\pi/N)$, $(A_4, a_{4,0}, a_{4,1}, a_{4,2}) = (0.125, 0, 0.6\pi, -0.3\pi/N)$, $(A_5, a_{5,0}, a_{5,1}, a_{5,2}) = (0.0625, 0, 0.3\pi, -0.2\pi/N)$, respectively.

Figs. 6(a) and 6(b) show the MSE of the chirp-rate estimates for the first and second LFM components, using the CPF-based, the ICPF-based estimators, and the MLE, respectively, together with the multi-component cancelation procedure. The SNR shown is the first component's SNR. For the CPF-based estimation, the time index is chosen at the middle point of observations where no spurious peaks appear. As seen from these figures, the ICPF-based estimator achieves similar performance as the MLE and outperforms the CPF-based estimator. The latter approaches the CRB only at high SNRs.

C. LFM Signal Detection

To compare the performance of the GLRT/RWT-based, RAT-based and ICPF-based detectors, an LFM signal is generated using parameters $a_0 = 0.1\pi$, $a_1 = 0.2\pi$, $a_2 = 0.1\pi/N$ and $n_0 = 0$. Due to the nonlinear transformation, analytical expressions of the probability of detection and probability of false alarm cannot be derived in closed form. Here, the simulated probability of detection versus SNR for a given probability of false alarm is shown in Fig. 7, where $N = 64$. It is shown that the ICPF-based detector provides a close detection performance as the GLRT/RWT-based detector, while the RAT-based detector provides worse results which may be attributed to the coordinate transformation and Polar line integrals. Specifically, compared to the GLRT/RWT-based detector, the ICPF-based detector shows about 0.5 dB performance loss, but saves in computational complexity from the 2-D searchto the

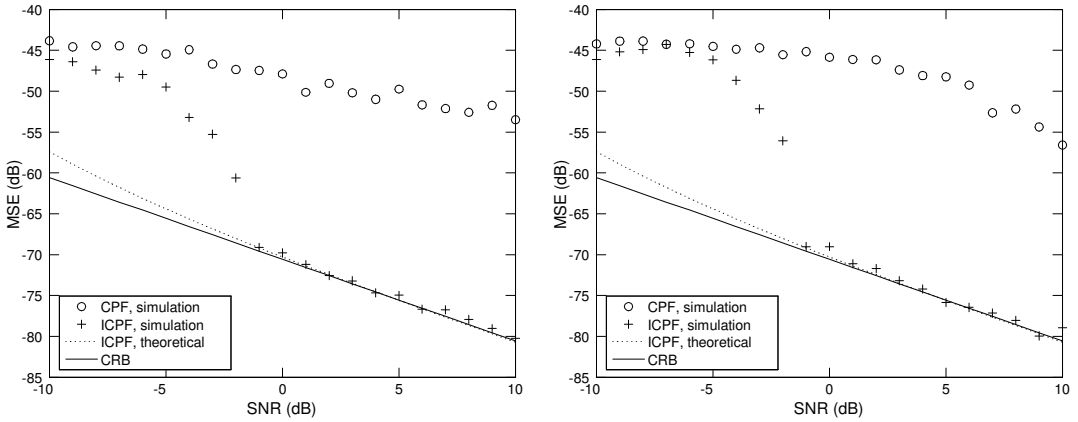

Fig. 5. MSE for the a_2 estimate of a 2-component LFM signal, (a) the first component; (b) the second component, when $N = 64$.

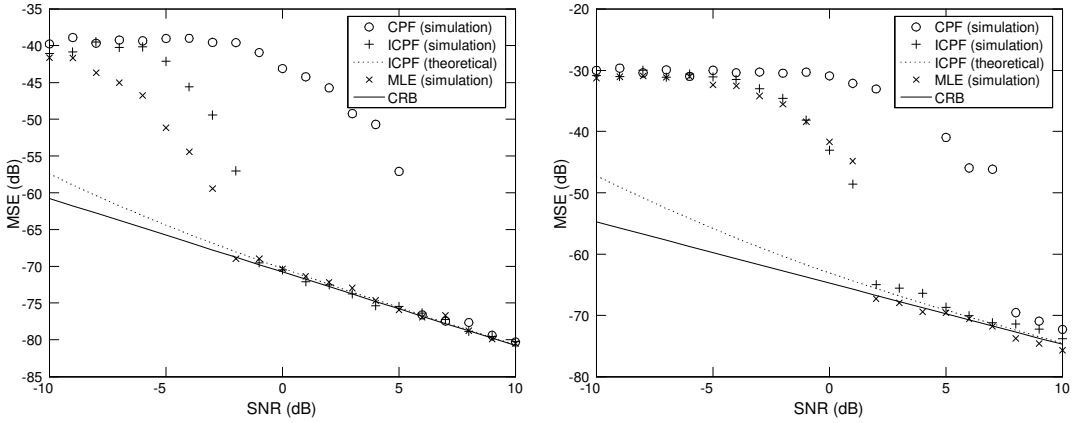

Fig. 6. MSE for the a_2 estimate of a 5-component LFM signal with varying component SNRs, (a) the first component; (b) the second component, when $N = 64$.

1-D search.

To verify the theoretical output SNR of the ICPF-based detector, an LFM signal with the same parameters as in the above example is simulated, except that $N = 256$. Fig. 8 shows the output SNR obtained from the Monte-Carlo simulation for the three squared-form detectors as well as their theoretical output SNR. It is observed that the simulated output SNR for the ICPF-based detector conforms to the theoretical expression in (19). Moreover, the detection performance for the three detectors are almost the same in terms of the output SNR.

VII. Conclusion

The ICPF has been proposed for LFM signal analysis. For either single- or multi-component LFM signals, the ICPF-based approach provides improved estimation accuracy and better capability of rejecting the interference than the CPF-based approach. Perfor-

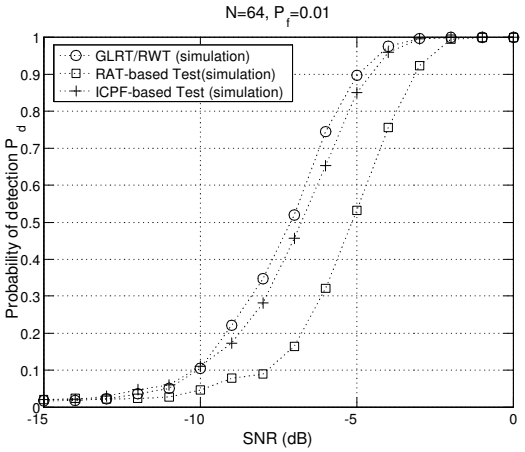

Fig. 7. Probability of detection versus SNR when probability of false alarm is fixed to 0.01 and $N = 64$.

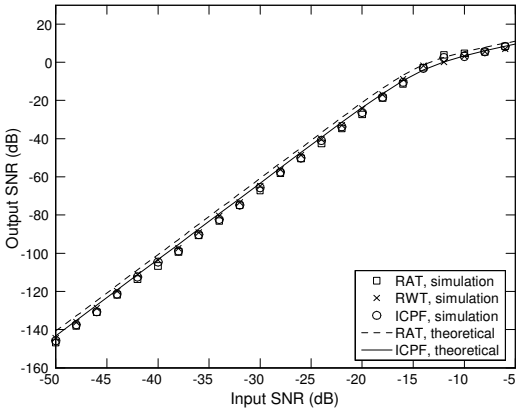

Fig. 8. The output SNR for the squared RAT, RWT and ICPF when $N = 256$.

mance analysis has been carried out in terms of the asymptotic bias and MSE for the estimation problem and the output SNR and SNR threshold for the detection problem. Comparison with other approaches including the MLE for the estimation and the GLRT for the detection shows the ICPF provides a reliable and computationally efficient tool for LFM signal detection and estimation.

Appendices

I. Asymptotic Bias and MSE

A. Chirp-Rate Parameter Estimate

We follow a first-order perturbation analysis as used in [7] for LFM signal estimation. Let $g_N(\Omega)$ be a noise-free function depending on Ω and N. A random perturbation $\delta g_N(\Omega)$ moves the global maximum Ω_0 of the $g_N(\Omega)$ to the point $\Omega_0 + \delta\Omega$. For the ICPF-based parameter estimator, the random perturbation is due to interference including cross-terms and noise-related terms. To derive the MSE of the ICPF-based estimates, let $g_N(\Omega)$ and $\delta g_N(\Omega)$ be

$$g_N(\Omega) = \sum_n \sum_m \sum_l s_1 s_2 s_3^* s_4^* e^{-j\Omega\left(m^2 - l^2\right)}, \tag{21}$$

$$\delta g_N(\Omega) \approx \sum_n \sum_m \sum_l z_{vs} e^{-j\Omega\left(m^2 - l^2\right)}, \tag{22}$$

where $s_1 = s(n+m), s_2 = s(n-m), s_3 = s(n+l)$, $s_4 = s(n-l)$ for notation simplicity, and z_{vs} includes the interference with no more than two noise terms due to the high SNR assumption:

$$\begin{aligned} z_{vs} \approx\ & s_1 s_2 s_3^* v_4^* + s_1 s_2 s_4^* v_3^* + s_1 s_3^* s_4^* v_2 \\ & + s_2 s_3^* s_4^* v_1 + s_1 s_2 v_3^* v_4^* + s_1 s_3^* v_2 v_4^* \\ & + s_1 s_4^* v_2 v_3^* + s_2 s_3^* v_1 v_4^* + s_2 s_4^* v_1 v_3^* + s_3^* s_4^* v_1 v_2, \end{aligned} \tag{23}$$

where $\{v_i\}_{i=1}^4$ are defined similarly as $\{s_i\}_{i=1}^4$ from the noise samples.

By definition of the maximum, we have

$$\frac{\partial \left[g_N(\Omega) + \delta g_N(\Omega)\right]}{\partial \Omega}\Big|_{\Omega_0 + \delta\Omega} = 0. \tag{24}$$

By using a first-order approximation, the above equation can be approximated as:

$$\frac{\partial g_N(\Omega_0)}{\partial \Omega} + \frac{\partial \delta g_N(\Omega_0)}{\partial \Omega} + \frac{\partial^2 g_N(\Omega_0)}{\partial \Omega^2}\delta\Omega \approx 0. \tag{25}$$

The first term is zero since Ω_0 maximizes $g_N(\Omega)$. Therefore, the estimation error $\delta\Omega$ can be expressed as

$$\delta\Omega = -\frac{\alpha}{\beta}, \tag{26}$$

where $\alpha = \frac{\partial \delta g_N(\Omega_0)}{\partial \Omega}$ and $\beta = \frac{\partial^2 g_N(\Omega_0)}{\partial \Omega^2}$. By using the derivatives of (21) and (22) in the above equation, we have

$$\alpha = \sum_n \sum_m \sum_l \left(m^2 - l^2\right) z_{vs} e^{-j\Omega_0\left(m^2-l^2-\pi/2\right)}, \tag{27}$$

$$\beta \approx -A^4 \frac{N^7}{630}. \tag{28}$$

Taking the expectation on (26) yields

$$E\{\delta\Omega\} = -\frac{E\{\alpha\}}{\beta} = 0, \tag{29}$$

due to the fact that

$$E\{\alpha\} \approx -2A^2\sigma^2 \left\{ \sum_n \sum_m \sum_l \left(m^2 - l^2\right) \right.$$

$$\left. [\delta(m-l) + \delta(m+l)] \right\} = 0, \tag{30}$$

where $\delta(n)$ indicates the Kronecker delta function. Hence, the chirp-rate estimate is asymptotically *unbiased* as a first-order approximation.

According to (26), the variance of $\delta\Omega$ can be expressed as

$$E\left\{|\delta\Omega|^2\right\} = \frac{E\{\alpha\alpha^*\}}{\beta^2}. \tag{31}$$

Based on the high-order moment properties of the Gaussian random variable [28], we have the following types of intermediate results

$$s_1 s_2 s_3^* s_5^* s_6^* s_7 E\{v_4^* v_8\} e^{j\Omega_0\left[\left(m_2^2-l_2^2\right)-\left(m^2-l^2\right)\right]}$$

$$= A^6\sigma^2\delta(n-l-n_2+l_2),$$

$$s_1 s_2 s_5^* s_6^* E\{v_3^* v_4^* v_7 v_8\} e^{j\Omega_0\left[\left(m_2^2-l_2^2\right)-\left(m^2-l^2\right)\right]}$$

$$= A^4\sigma^4\delta(n+l-n_2-l_2)\,\delta(n-l-n_2+l_2)$$

$$+A^4\sigma^4\delta(n+l-n_2+l_2)\,\delta(n-l-n_2-l_2), \tag{32}$$

where $s_5 = s(n_2+m_2), s_6 = s(n_2-m_2), s_7 = s(n_2+l_2)$, $s_8 = s(n_2-l_2)$ and $\{v_i\}_{i=5}^8$ are similarly defined. Based on the above results and (27), $E\{\alpha\alpha^*\}$ can be computed as multiple summations of the delta functions in (32) and the results are approximated as

$$E\{\alpha\alpha^*\} \approx A^6\sigma^2\left(\frac{8N^9}{8744}\right) +$$

$$+A^4\sigma^4\left(\frac{4N^8}{1440} + \frac{16N^8}{4033}\right). \tag{33}$$

Using the above equation in (31), we have

$$E\left\{|\delta\Omega|^2\right\} \approx \frac{363}{\mathrm{SNR}N^5} + \frac{2677}{\mathrm{SNR}^2N^6}. \tag{34}$$

Since $\Omega = 2a_2$, the mean-square value of δa_2 is

$$E\left\{(\delta a_2)^2\right\} = \frac{90}{N^5}\left(\frac{1.008}{\mathrm{SNR}} + \frac{7.433}{\mathrm{SNR}^2N}\right). \tag{35}$$

B. Frequency Parameter Estimate

The dechirped signal can be expressed as

$$x_d(n) = x(n)\,e^{-j\hat{a}_2 n^2} = x(n)\,e^{-j(a_2+\delta a_2)n^2}$$

$$= [s(n) + v(n)]\,e^{-j(a_2+\delta a_2)n^2}$$

$$= \left[Ae^{j(a_0+a_1 n)} + v(n)\,e^{-ja_2n^2}\right] e^{-j\delta a_2 n^2}. \tag{36}$$

Since δa_2 is of order $N^{-5/2}$ (see (35)) and $\delta a_2 n^2$ is of order $N^{-1/2}$ for all n, the following approximation holds for large N [7]

$$e^{-j\delta a_2 n^2} \approx 1 - j(\delta a_2)\,n^2. \tag{37}$$

By using (37), the dechirped signal can be approximated as

$$x_d(n) = Ae^{j(a_0+a_1 n)} +$$

$$\left[v(n)\left(1 - j(\delta a_2)\,n^2\right)e^{-ja_2n^2}\right.$$

$$\left. - Ae^{j(a_0+a_1 n)} j(\delta a_2)\,n^2\right]. \tag{38}$$

Once again, we apply a first-order perturbation analysis to the a_1 estimate, which is the

frequency location maximizing the magnitude squared DFT of $x_d(n)$:

$$g_N(\omega) = \sum_n A e^{j(a_0+a_1 n)} e^{-j\omega n}, \tag{39}$$

$$\delta g_N(\omega) = \sum_n \left[v(n)\left(1 - j(\delta a_2) n^2\right) e^{-j a_2 n^2} - A e^{j(a_0+a_1 n)} j(\delta a_2) n^2 \right] e^{-j\omega n}, \tag{40}$$

The functions $g_N(\omega)$, $\delta g_N(\omega)$, and their derivatives at the point of the global maximum $\omega_0 = a_1$, are given by

$$g_N(\omega_0) = A e^{j a_0} N,$$

$$\frac{\partial g_N(\omega_0)}{\partial \omega} = -jA e^{j a_0} \sum_n n \approx 0,$$

$$\frac{\partial^2 g_N(\omega_0)}{\partial \omega^2} = -A e^{j a_0} \sum_n n^2 \approx -A e^{j a_0} \frac{N^3}{12}, \tag{41}$$

$$\begin{aligned} &\delta g_N(\omega_0) = \\ &= \sum_n \left[v(n)\left(1 - j(\delta a_2) n^2\right) e^{-j\left(a_1 n + a_2 n^2\right)} \right. \\ &\left. - jA e^{j a_0} (\delta a_2) n^2 \right] \\ &\approx \sum_n v(n)\left(1 - j(\delta a_2) n^2\right) e^{-j\left(a_1 n + a_2 n^2\right)} \\ &- jA e^{j a_0} (\delta a_2) \frac{N^3}{12}, \end{aligned} \tag{42}$$

$$\begin{aligned} &\frac{\partial \delta g_N(\omega_0)}{\partial \omega} = \\ &= -j \sum_n n \left[v(n)\left(1 - j(\delta a_2) n^2\right) e^{-j\left(a_1 n + a_2 n^2\right)} \right. \\ &\left. - A e^{j a_0} j(\delta a_2) n^2 \right] \\ &\approx -j \sum_n n v(n)\left(1 - j(\delta a_2) n^2\right) e^{-j\left(a_1 n + a_2 n^2\right)}. \end{aligned} \tag{43}$$

By utilizing the first-order analysis for the complex sinusoid signal in [7] along with the above equations, we obtain

$$\begin{aligned} \alpha &= 2\Re\left\{ g_N(\omega_0) \frac{\partial^2 g_N^*(\omega_0)}{\partial \omega^2} \right\} \\ &\quad + 2\Re\left\{ + \frac{\partial g_N(\omega_0)}{\partial \omega} \frac{\partial g_N^*(\omega_0)}{\partial \omega} \right\} \\ &= -A^2 \frac{N^4}{6}, \end{aligned} \tag{44}$$

$$\begin{aligned} \beta =& 2\Re\left\{ g_N(\omega_0) \frac{\partial \delta g_N^*(\omega_0)}{\partial \omega} \right\} \\ &+ 2\Re\left\{ \frac{\partial g_N(\omega_0)}{\partial \omega} \delta g_N^*(\omega_0) \right\} \\ &\approx 2N\Re\left\{ -j\left(\sum_n n s(n) v^*(n) \right.\right. \\ &\left.\left. + \sum_n n^3 s(n) v^*(n) j(\delta a_2) \right) \right\} \\ =& 2N\left(\Im\{\eta\} + \Im\{\gamma\}\right), \end{aligned} \tag{45}$$

where η and γ represent the first and second summations in (45), respectively.

Substituting (26) into the above equations yields the following results:

$$E\left\{ (\Im[\eta])^2 \right\} \approx \frac{A^2 \sigma^2 N^3}{24}, \tag{46}$$

$$E\{\eta^* \gamma\} = 2E\{\eta\gamma\} \approx \sigma^4, \tag{47}$$

$$E\{\gamma\gamma\} = 0, \tag{48}$$

$$E\{\gamma\gamma^*\} \approx \frac{\sigma^4 N^2}{3}. \tag{49}$$

Hence,

$$\begin{aligned} E\left\{\beta^2\right\} =& 4N^2 \left[E\left(\Im[\eta]^2\right) + E\left(\Im[\eta]\Im\{\gamma\}\right) \right. \\ &\left. + E\left(\Im\{\gamma\}^2\right) \right] \\ \approx& 4N^2 \left[\frac{A^2\sigma^2 N^3}{24} + \frac{\sigma^4 N^2}{6} \right]. \end{aligned} \tag{50}$$

Finally, the asymptotic MSE of the a_1 estimate is

$$\begin{aligned} E\left\{(\delta a_1)^2\right\} &= \frac{E\left\{\beta^2\right\}}{\alpha^2} \\ &\approx \frac{6}{N^3 \mathrm{SNR}} \left(1 + \frac{4}{N \mathrm{SNR}}\right). \end{aligned} \tag{51}$$

C. Phase and Amplitude Parameter Estimates

We now derive the asymptotic MSE of the a_0 and A estimates using the estimation procedure described in Section III. According to (10) and (11), the dechirping technique is used again. Similar to the approximation used in (37), the dechirped signal can be expressed as

$$\begin{aligned} x_{d_2}(n) =& Ae^{ja_0}\left[1+A^{-2}s^*(n)\,v(n)\right] \\ &\times\left(1-j(\delta a_1)\,n-j(\delta a_2)\,n^2\right) \\ \approx& Ae^{ja_0}\Big[1+A^{-2}s^*(n)\,v(n) \\ &-j(\delta a_1)\,n-j(\delta a_2)\,n^2\Big]. \end{aligned} \tag{52}$$

Let $\vartheta=\frac{1}{N}\sum_n x_{d_2}$. We have

$$\begin{aligned} \log\vartheta =& \log\left\{Ae^{ja_0}\Big[1+\frac{1}{A^2N}\sum_n s^*(n)\,v(n) \right. \\ &\left. -j(\delta a_2)\frac{N^2}{12}\Big]\right\} \\ \approx& \log A+ja_0+ \\ &+\frac{1}{A^2N}\sum_n s^*(n)\,v(n)-j\frac{\delta a_2N^2}{12}. \end{aligned} \tag{53}$$

Using $\hat{A}=e^{\Re\{\log(\vartheta)\}}$ in (11) yields

$$\log\hat{A}=\log A+\Re\left\{\frac{1}{A^2N}\sum_n s^*(n)\,v(n)\right\}. \tag{54}$$

Since $\log\hat{A}=\log\left[A(1+\delta A/A)\right]\approx\log A+\delta A/A$ [7], the estimation error of A can be expressed as

$$\delta A\approx\frac{1}{NA}\Re\left\{\sum_n s^*(n)\,v(n)\right\}. \tag{55}$$

Then the MSE of the amplitude estimate is

$$E\left\{(\delta A)^2\right\}=\frac{1}{N^2A^2}\frac{A^2\sigma^2N}{2}=\frac{\sigma^2}{2N}. \tag{56}$$

Meanwhile, the estimate of a_0 can be expressed as

$$\begin{aligned} \hat{a}_0 =& \Im\{\log\vartheta\} \\ =& a_0+\frac{1}{NA^2}\Im\left\{\sum_n s^*(n)\,v(n)\right\}-\frac{\delta a_2N^2}{12}. \end{aligned} \tag{57}$$

Therefore, the MSE of the a_0 estimate is

$$\begin{aligned} E\left\{(\delta a_0)^2\right\}\approx& \frac{1}{2N\mathrm{SNR}}+\frac{1}{144}N^4E\left\{(\delta a_2)^2\right\}-0 \\ \approx& \frac{1.13}{N\mathrm{SNR}}+\frac{4.65}{N^2\mathrm{SNR}^2}. \end{aligned} \tag{58}$$

II. Output SNR Analysis

With signal only, the test statistic in (17) at the maximum point $\Omega_0=2a_2$ is

$$\begin{aligned} &\mathrm{ICPF}_s(\Omega_0)= \\ &\quad A^4\sum_n\sum_m\sum_l s_1s_2s_3^*s_4^*e^{-j\Omega_0(m^2-l^2)} \\ &\quad =A^4\sum_{n=0}^{N-1}\sum_m\sum_l 1 \\ &\quad =A^4\frac{N^3+2N}{3}\approx A^4\frac{N^3}{3}, \end{aligned} \tag{59}$$

where we consider the case where the observation time is $n=0,1,\cdots,N-1$ in order to compare with the output SNR results of the RWT and RAT [9,13], m and l are subject to the constraint accordingly, and the last approximation is valid for $N\gg1$. The output SNR for the case $n=-(N-1)/1,\cdots,0,\cdots,(N-1)/2$ can be similarly obtained. When the signal is corrupted by noise, the expectation of $\mathrm{ICPF}_x(\Omega_0)$ can be expressed by exploiting the moment properties of a complex Gaussian random variable [28]

$$\begin{aligned} &E\{\mathrm{ICPF}_x(\Omega_0)\} \\ &=\sum_n\sum_m\sum_l\Big\{s_1s_2s_3^*s_4^*+s_1s_3^*E\{v_2v_4^*\} \\ &+s_1s_4^*E\{v_2v_3^*\}+s_2s_3^*E\{v_1v_4^*\}+s_2s_4^*E\{v_1v_3^*\} \\ &+E\{v_1v_2v_3^*v_4^*\}\Big\}e^{-j\Omega_0(m^2-l^2)}. \end{aligned} \tag{60}$$

Using the following results,

$$\begin{aligned}
s_1 s_2 s_3^* s_4^* e^{-j\Omega_0\left(m^2-l^2\right)} &= A^4 \\
s_1 s_3^* E\left\{v_2 v_4^*\right\} e^{-j\Omega_0\left(m^2-l^2\right)} &= A^2\sigma^2\delta\left(m-l\right) \\
s_1 s_4^* E\left\{v_2 v_3^*\right\} e^{-j\Omega_0\left(m^2-l^2\right)} &= A^2\sigma^2\delta\left(m+l\right) \\
s_2 s_3^* E\left\{v_1 v_4^*\right\} e^{-j\Omega_0\left(m^2-l^2\right)} &= A^2\sigma^2\delta\left(m+l\right) \\
s_2 s_4^* E\left\{v_1 v_3^*\right\} e^{-j\Omega_0\left(m^2-l^2\right)} &= A^2\sigma^2\delta\left(m-l\right) \\
E\left\{v_1 v_2 v_3^* v_4^*\right\} e^{-j\Omega_0\left(m^2-l^2\right)} &= \sigma^4\left[\delta\left(m-l\right)\right] \\
&\quad + \sigma^4\left[\delta\left(m+l\right)\right],
\end{aligned} \tag{61}$$

we can express (60) as

$$\begin{aligned}
&E\left\{\mathrm{ICPF}_x(\Omega_0)\right\} = \\
&= \sum_n \sum_m \sum_l \Big\{ A^4 + \left(2A^2\sigma^2 + \sigma^4\right) \\
&\times \left[\delta(m+l) + \delta(m-l)\right] \Big\} \\
&\approx A^4\frac{N^3}{3} + 2A^2\sigma^2N^2 + \sigma^4N^2.
\end{aligned} \tag{62}$$

The second-order moment is

$$\begin{aligned}
&E\left\{\left|\mathrm{ICPF}_x\left(\Omega_0\right)\right|^2\right\} \\
&= \sum_n \sum_m \sum_l \sum_{n_2} \sum_{m_2} \sum_{l_2} E\Big\{ \left(s_1+v_1\right)\left(s_2+v_2\right) \\
&\left(s_3^*+v_3^*\right)\left(s_4^*+v_4^*\right)\left(s_5^*+v_5^*\right)\left(s_6^*+v_6^*\right) \\
&\left(s_7+v_7\right)\left(s_8+v_8\right) \Big\} e^{j\Omega_0\left[\left(m_2^2-l_2^2\right)-\left(m^2-l^2\right)\right]}.
\end{aligned} \tag{63}$$

By using the properties shown in (61), (63) can be simplified as multiple summations of delta functions and the results are

$$\begin{aligned}
&E\left\{\left|\mathrm{ICPF}_x\left(\Omega_0\right)\right|^2\right\} \\
&= A^8\frac{N^6}{9} + A^6\sigma^2\left(\frac{67}{30}N^5\right) + \\
&+ A^4\sigma^4\left(\frac{2}{3}N^5 + \frac{71}{6}N^4\right) \\
&+ A^2\sigma^6\left(4N^4 + \frac{64}{3}N^3\right) + \sigma^8\left(N^4 + 4N^3\right).
\end{aligned} \tag{64}$$

Combining (60) and (64), the variance can be obtained as

$$\begin{aligned}
\mathrm{var}\left\{\mathrm{ICPF}_x(\Omega_0)\right\} =& \frac{9}{10}A^6\sigma^2N^5 + \frac{47}{6}A^4\sigma^4N^4 \\
&+ \frac{64}{3}A^2\sigma^6N^3 + 4\sigma^8N^3.
\end{aligned} \tag{65}$$

Substituting (59) and (65) in (18) yields (19).

References

[1] A. W. Rihaczek, *Principles of high-resolution radar*, McGraw-Hill, New York, 1969.

[2] B. Porat, *Digital processing of random signals: theory and methods*, Prentice Hall, Englewood Cliffs, NJ, 1994.

[3] J. C. Curlandar and R. N. McDonough, *Synthetic Aperture Radar - System and Signal Processing*, John Wiley & Sons, New York, 1991.

[4] D. R. Wehner, *High-Resolution Radar*, Artech House, Norwood, MA, 1995.

[5] T. Abotzoglou, "Fast maximum likelihood joint estimation of frequency and frequency rate," *IEEE Trans. on Aerosp. Electron. Syst.*, vol. 22, pp. 708–715, November 1986.

[6] P. M. Djuric and S. Kay, "Parameter estimation of chirp signals," *IEEE Trans. Signal Processing*, vol. 38, no. 12, pp. 2118–2126, December 1990.

[7] S. Peleg and B. Porat, "Linear FM signal parameter estimation from discrete-time observations," *IEEE Trans. Aerosp. Electron. Syst.*, vol. 27, no. 4, pp. 607–614, July 1991.

[8] J. C. Wood and D. T. Barry, "Radon transformation of time-frequency distributions for analysis of multicomponent signals," *IEEE Trans. Signal Processing*, vol. 42, no. 11, pp. 3166–3177, November 1994.

[9] S. Barbarossa, "Analysis of multicomponent LFM signals by a combined Wigner-Hough transform," *IEEE Trans. Signal Processing*, vol. 43, no. 6, pp. 1511–1515, June 1995.

[10] B. Friedlander and J. M. Francos, "Estimation of amplitude and phase parameters of multicomponent signals," *IEEE Trans. Signal Processing*, vol. 43, no. 4, pp. 917–926, April 1995.

[11] S. Peleg and B. Friedlander, "Multicomponent signals analysis using the polynomial-phase transform," *IEEE Trans. Aerosp. Electron. Syst.*, vol. 32, no. 1, pp. 378–387, January 1996.

[12] S. Barbarossa, A. Scaglione, and G. Giannakis, "Product high-order ambiguity function for mulit-component polynomial phase signal modeling," *IEEE Trans. Signal Processing*, vol. 46, no. 3, pp. 691–708, March 1998.

[13] M. Wang, A. K. Chan, and C. K. Chui, "Linear frequency-modulated signal detection using Radon-Ambiguity transform," *IEEE Trans. Signal Processing*, vol. 46, no. 3, pp. 571–586, March 1998.

[14] X.-G. Xia, "Discrete Chirp-Fourier transform and its applicationto chirp rate estimation," *IEEE Trans. Signal Processing*, vol. 48, no. 11, pp. 3122–3133, November 2000.

[15] B. Volcker and B. Ottersten, "Chirp parameter estimation from a sample covariance matrix,"

IEEE Trans. Signal Processing, vol. 49, no. 3, pp. 603–612, March 2001.

[16] P. Wang and J. Yang, "Multicomponent chirp signals analysis using product cubic phase function," *Digital Signal Processing*, vol. 16, no. 6, pp. 654–669, November 2006.

[17] D. S. Pham and A. M. Zoubir, "Analysis of multicomponent polynomial phase signals," *IEEE Trans. Signal Processing*, vol. 55, no. 1, pp. 56–65, January 2007.

[18] K. S. Kulpa, "Focusing range image in VCO based FMCW radar," in *Proceedings of 2003 International Radar Conference*, Adelaide, Australia, September 2003.

[19] P. O'Shea, "A fast algorithm for estimating the parameters of a quadratic FM signal," *IEEE Trans. Signal Processing*, vol. 52, no. 2, pp. 385–393, February 2004.

[20] P. Wang, I. Djurović, and J. Yang, "Generalized high-order phase function for parameter estimation of polynomial phase signal," *IEEE Trans. Signal Processing*, vol. 56, no. 7, pp. 3023–3028, July 2008.

[21] S. Peleg and B. Friedlander, "The discrete polynomial-phase transform," *IEEE Trans. Signal Processing*, vol. 43, no. 8, pp. 1901–1914, August 1995.

[22] C. De Luigi and C. Jauffret, "Estimation and classification of FM signals using time frequency transforms," *IEEE Trans. Aerosp. Electron. Syst.*, vol. 41, no. 2, pp. 421–437, April 2005.

[23] S. Barbarossa and V. Petrone, "Analysis of polynomial phase signals by an integrated generalized ambiguity function," *IEEE Trans. Signal Processing*, vol. 47, no. 2, pp. 316–327, February 1997.

[24] B. Porat and B. Friedlander, "Asymptotic statistical analysis of the high-order ambiguity function for parameter estimation of polynomial-phase signals," *IEEE Trans. Info. Theory*, vol. 42, no. 3, pp. 995–1001, May 1996.

[25] W. Li, "Winger distribution method equivalent to a dechirp method for detecting a chirp signal," *IEEE Trans. Acoust. Speech, Signal Processing*, vol. 35, no. 8, pp. 1210–1211, August 1987.

[26] S. M. Kay, *Fundamental of Statistical Signal Processing: Estimation Theory*, Prentice Hall, Upper Saddle River, NJ, 1998.

[27] B. Ristic and B. Boashash, "Comments on "the Cramer-Rao Lower Bounds for signals with constant amplitude and polynomial phase"," *IEEE Trans. Signal Processing*, vol. 46, no. 6, pp. 1708–1709, June 1998.

[28] I. S. Reed, "On a moment theorem for complex gaussian processes," *IRE Trans. Info. Theory*, vol. 8, pp. 194–195, April 1962.